Volume 18, Number 5, 2025. pp. 659-667

Jordan Journal of Physics

ARTICLE

Gas Sensing Performance of ZnO/Si Nanostructured Thin Films Synthesis by Spin-Coating

Ahmad Z. Al-Jenaby, Othman A. Fahad, Saadallah F. Hasan and **Abubaker. S. Mohammed**

Ministry of Education, Directorate of Education in Al-Anbar, Al-Anbar, Iraq.

Doi: **https://doi.org/10.47011/18.5.8**

Received on: 11/01/2025; *Accepted on: 23/04/2025*

Abstract: In this work, ethanol, ammonium hydroxide, and a zinc acetate-containing precursor solution were used to create zinc oxide (ZnO) nanostructured films on silicon substrates using the spin-coating technique. The study also investigated how several layers affect structural, optical, and sensing properties. X-ray revealed that ZnO nanoparticles had a hexagonal structure phase and were polycrystalline, with the (002) plane as the preferred orientation parallel to the substrate surface. According to AFM analysis, as the number of layers increased, the grain size decreased, and the surface roughness increased. The energy gap increased from 3.31 to 3.39 eV as the number of layers increased, according to UV-visible analysis. Sensitivity of the films to ammonia gas in a 50 ppm concentration range was assessed at working temperatures ranging from room temperature to 150 °C. Nanostructured ZnO thin films must be produced for efficient and reasonably priced gas sensing applications. A synergistic effect was observed in this study: reducing grain size, increasing operating temperature, and enhancing surface roughness improved sensitivity, reaching up to 140.7% when seven layers were applied.

Keywords: ZnO nanoparticles, Sensitivity, Grain size, Roughness, NH3 gas sensor.

1. Introduction

Current solid-state device technologies have a wide range of applications. Among the materials that have received extensive investigation in recent years are transparent conductive oxides (TCOs) in thin films [1]. Zinc oxide (ZnO) is one of the most significant semiconductor materials, exhibiting a hexagonal crystal structure (wurtzite) and belonging to group II–VI compounds [2]. The compound has a direct band gap of 3.2–3.4 eV, is abundant, cheap, non-toxic, and has n-type conductivity [3]. Its visible range optical transmission is good, making it suitable for the solar spectrum [4, 5]. It has a variety of uses in optoelectronic devices due to its structural, electrical, and optical properties [4, 6]. By increasing the number of layers, zinc oxide films can be used to improve sensing and electrical properties, among other things, to increase ammonia gas sensitivity [7]. Gas sensing is influenced not only by structural properties, including grain size, grain boundaries, and surface-to-volume ratio, but also by surface states and oxygen adsorption rates [8–11]. Multilayered ZnO thin films can be deposited using a variety of techniques, including PLD [12], sputtering [13, 14], and spray pyrolysis [15]. The spin coating method is the most straightforward, economical, and suitable for large-area deposition. A straightforward and affordable sol-gel deposition method was used to apply the characteristics of stacked ZnO thin film layers [16]. Reasonably priced optoelectronic device manufacturing will be made easier by the ongoing work. The novelty of this work lies in fabricating ZnO thin films with three, five, and seven layers on silicon substrates that operate at room temperature. By producing nanostructured films, the resulting gas sensor can function within broadband in different temperatures.

Corresponding Author: Othman Abed Fahad **Email**: Othmanabad2@gmail.com

The current work has examined structural, morphological, sensing, and optical properties of 3-, 5-, and 7-layer thin films made using a straightforward technique (sol-gel spin coating).

2. Experimental

The sol-gel spin coating method was used to prepare ZnO films for growth on silicon substrates. Zinc dehydrate [Zn $(CH_3COO)_2$-$2H_2O$] was dissolved in isopropanol [$(CH_3)_2CHOH$]. Monoethanolamide was used to stabilize the solution (MEA) [NH2 CH2CH2OH]. It was incorporated into a 25 mL solution at a rate of 1, in order to make a con. of 0.2 mol/l. To create uniformity, the solutions were stirred for one hour at 65 °C. Clear solutions were then allowed to age at room temperature for a full day. The silicon substrates were cleaned with ethanol and acetone for ten minutes each using an ultrasonic cleaner, and then dried following a cleaning with deionized water prior to the deposition process. A small amount of the prepared coating material in liquid form was applied by dropper to the center of the substrate fixed in the spin coating machine at 2500 rpm. This process was repeated several times to obtain multiple layers (3, 5, and 7). The films were heated in an oven at 250 °C for 5 minutes to remove organic residues and evaporate the solvent. Then, the films are annealed for 1 hour at 500 °C in air. The thickness of the deposited film was measured using an optical interferometer method based on interference between a He-Ne laser (632 nm) reflected from the substrate and the film surface. We call this the Fizeau approach. The thickness was computed using the formula. The films had thicknesses of roughly 100, 200, and 300 nm. The films were measured using a profilometer, in which part of the film is scratched to expose the substrate, and the device measures the height difference between the film surface and the exposed substrate.

3. Results and Discussion

Figure 1 shows probes of XRD patterns that provided information about film structure and were used to study the crystal structure of ZnO, recorded in the range between 20° and 80°. The observed peaks at (010), (002), and (011) appear in XRD patterns along with other peaks, demonstrating the hexagonal polycrystalline (wurtzite) structure of the ZnO thin films, as indicated on the card with the number [17]. The (002) peak was the most noticeable, suggesting a preferred growth direction along the c-axis. This proved that the surface free energy of the (002) planes was the most stable when compared to other planes. Among other things, the crystals' position, intensity, and preferred orientation can reveal details about their size, tension, and strain [18, 19]. For the three-layer ZnO film, the peak intensity was incredibly low. Increasing the number of layers from five to seven caused a steady increase in the density of the ZnO film. The figure illustrates how the number of layers increases from three to seven, resulting in a gradual increase in peak intensity, indicating higher film density. As the number of layers increased, the (002) peak also became sharper, suggesting improved crystallinity with increasing film thickness [20].

This behavior can be explained by competitive growth among adjacent crystallites based on their orientation. Crystals with energetically favorable orientations grow at the expense of others, leading to a dominant crystallographic orientation and improved overall crystallinity [21, 22]. This competitive growth mechanism likely accounts for the observed increase in crystallinity as the film thickness increased, as supported by the decreasing FWHM values [23,24]. The average crystallite sizes were calculated using Scherrer's equation. The crystallite size of the ZnO films decreased from 13.23 nm to 9.86 nm as the film thickness increased.

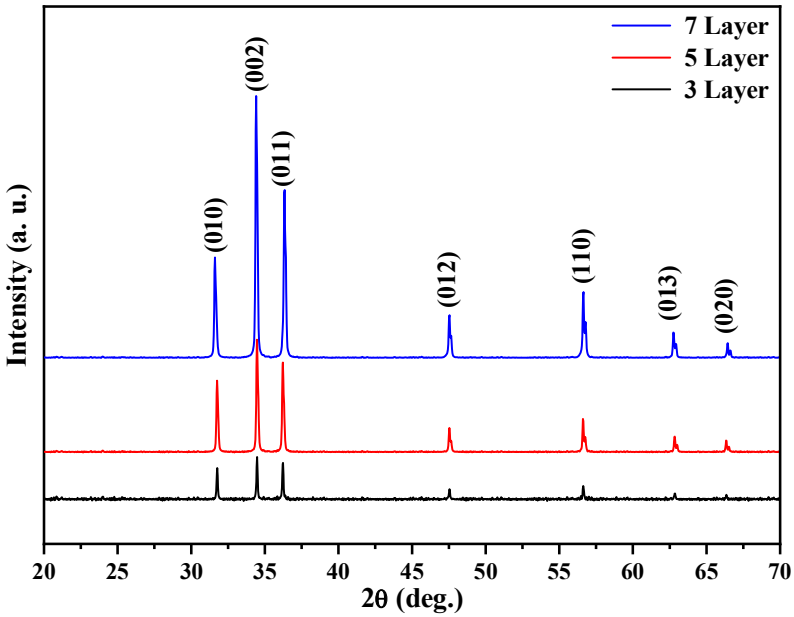

FIG. 1. XRD analysis of the generated ZnO for all films.

Figure 2 presents the surface topography of the annealed ZnO films, analyzed using AFM. The topographical analysis of surface roughness in two and three dimensions is displayed in Fig. 2(a). A 2.0 × 2.0 μm region was scanned from the AFM images of ZnO films. This indicates that the surface morphology is dominated by hexagonally faceted columnar granules. It is clear that the surface roughness of the films increased with their thickness. The 3L film thickness had a grain size of 99.41 nm and a root mean square (RMS) roughness of 2.17 nm; this suggests excellent homogeneity and good crystal regularity. As the number of layers increased to five and seven, the grain size decreased to 86.31 and 73.23 nm, while roughness progressively increased to 3.82 and 4.37 nm, respectively. The roughness increased as the ZnO thickness increased due to the decreasing grain size and the increased number of grains that formed [25, 26]. The high surface roughness of ZnO films makes them useful for gas sensors [27]. The sensitivity and response time of ZnO-based gas sensors are significantly impacted by the degree of roughness of the thin films. As thickness increased, so did the peak-to-peak and ten-point heights, according to Table 1, demonstrating the regularity of the generated films and the viability of using them as sensors, as improved absorption is achieved by surface uniformity [28]. Film roughness influences the sensor response by increasing the surface area specifically suited for gas adsorption [29]. To improve the gas sensor device, this increase is essential.

TABLE 1. AFM parameters of ZnO films with 3, 5, and 7 layers.

Sample ZnO layers	Ave. diameter (nm)	Roughness (nm)	R.M.S (nm)	Peak-peak (nm)	Ten-point hight (nm)
3 La.	99.41	2.17	2.36	11.48	6.28
5 La	86.31	3.82	4.22	14.29	12.77
7La.	75.23	4.37	4.83	18.32	12.57

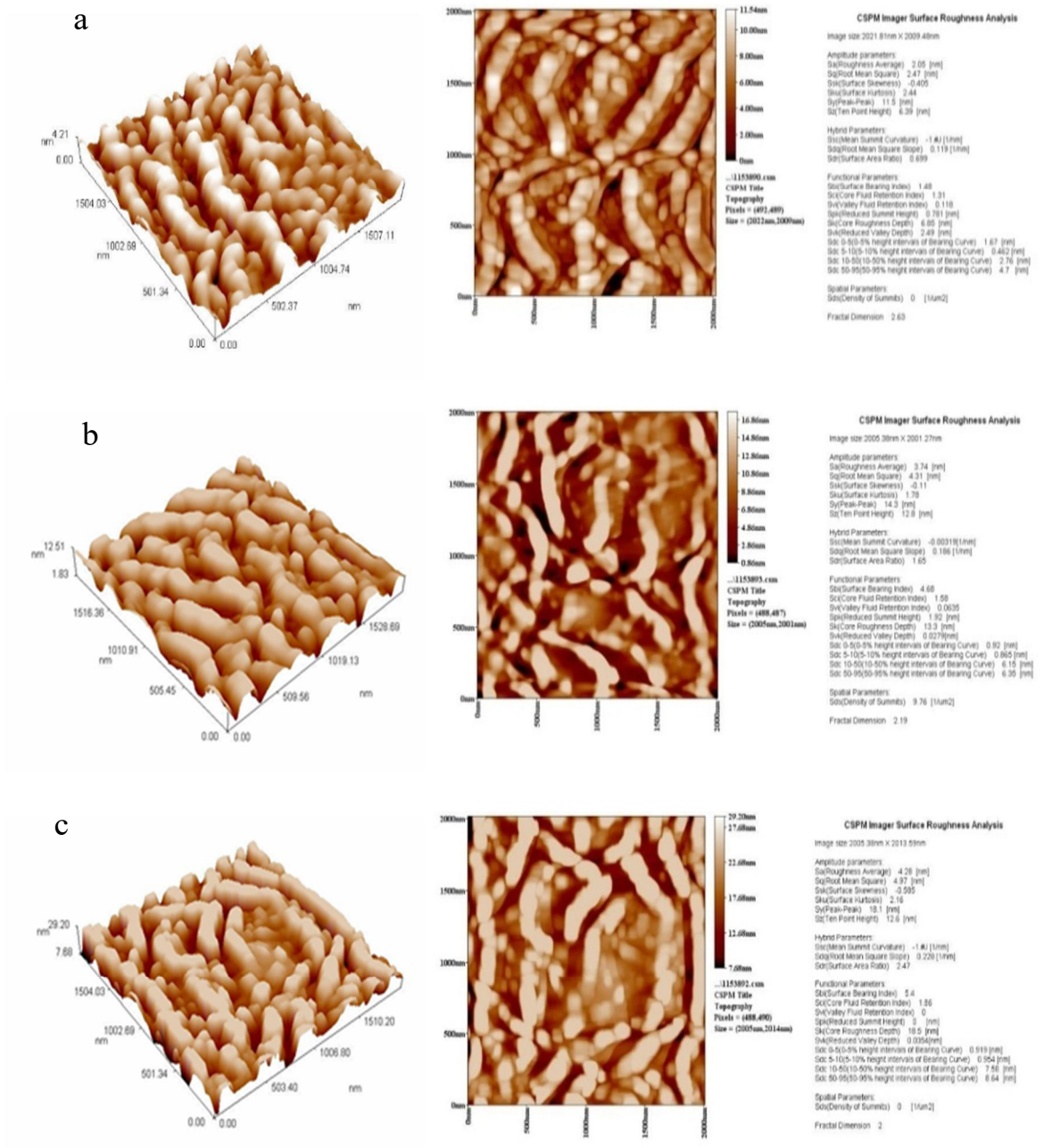

FIG. 2. AFM images of ZnO thin films with 3, 5, and 7 layers.

Figure 3 shows the transmittance spectra of ZnO films measured over the wavelength range of 200–1100 nm. The impact of layer count on ZnO film optical characteristics, including transmittance and band gap, was examined. The transmittance curves of ZnO films at different film thicknesses are shown in Fig 3. All of the samples exhibited good transparency, exceeding 84%. As the film thickness and surface roughness increased, the transmittance changed. This result was expected since when the thickness of a material increases, photons are absorbed into it in greater quantities. Additionally, the spectra revealed a shift in the absorption edge toward higher energies, which is associated with the thickness values. As the film thickness increased, the free spectral range decreased, resulting in more oscillations with the substrate [30]. Therefore, oscillations increased toward longer wavelengths. Interferences in the substrate are generally not observable in the incoherent formulation. However, it is well known that below the radiation wavelength of 500 nm (toward higher energy side of visible spectrum), the absorption coefficient of TCOs increases gradually and peaks at the ultraviolet (UV) region, resulting in the disappearance of interference patterns of the transmission

spectrum in this region (i.e., higher energy-side of the spectrum) [31, 32]. Since the absorbance increases with increasing thickness, the absorption coefficient decreases. Therefore, the phenomenon of optical quantum confinement is not achieved [24, 33]. Figure 4 shows the Tauc's plot for ZnO films as a function of film thickness. The band gap grew from 3.31 to 3.39 eV as the film thickness increased. As layer thickness increases, the optical band gap rises because of other lattice defects and a decreasing trend in strain. This is consistent with what Ennaceri, Houda, *et al.* found [34, 35]. The reduction in nanosize, which supports the charge carrier quantum confinement, may also be the cause of this [36, 37] and determines the band gap of the film (Fig. 4).

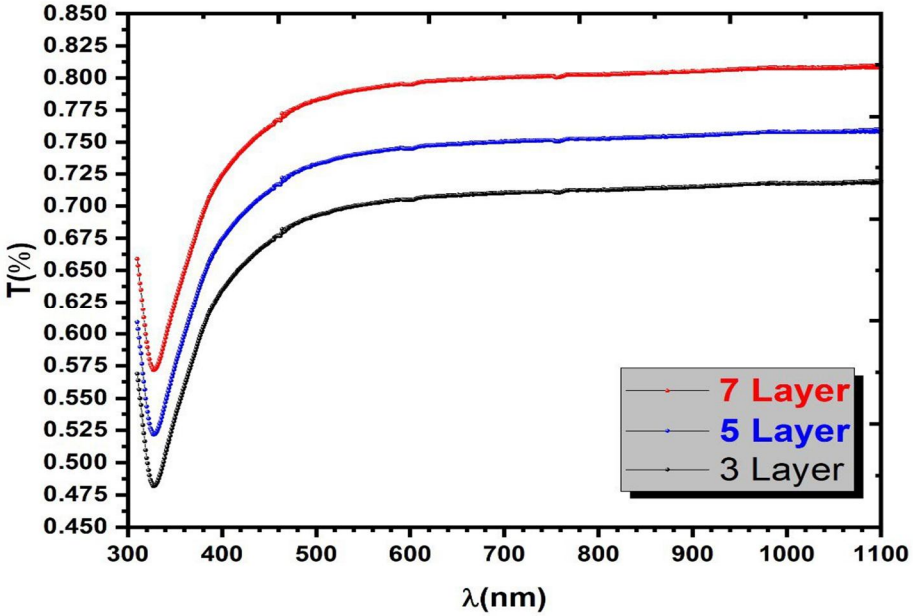

FIG. 3. The ZnO transmittance of all layers.

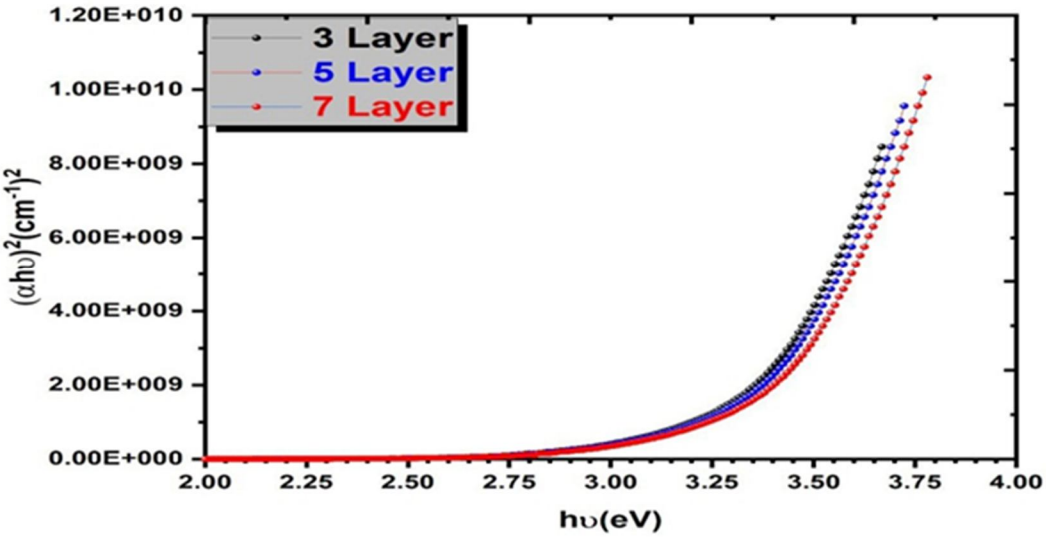

FIG. 4. The ZnO energy gap of all layers.

Figure 5 shows FE-SEM images of the surface for ZnO films on silicon papered by spin-coated with 3, 5, and 7 layers. Nanoparticles were formed on structure thin films. The image for FE-SEM shows height difference possibility in structures. As shown in Fig. 5(a), the ZnO film spin-coated with three layers shows less dense structure compared to the ZnO thin film spin-coated with five layers, depicted in Fig. 5(b). The ZnO thin film with seven layers, shown in Fig. 5(c), displays a more compact and uniform morphology with larger grains after annealing. This enhances the sensitivity characteristics of the gas sensor.

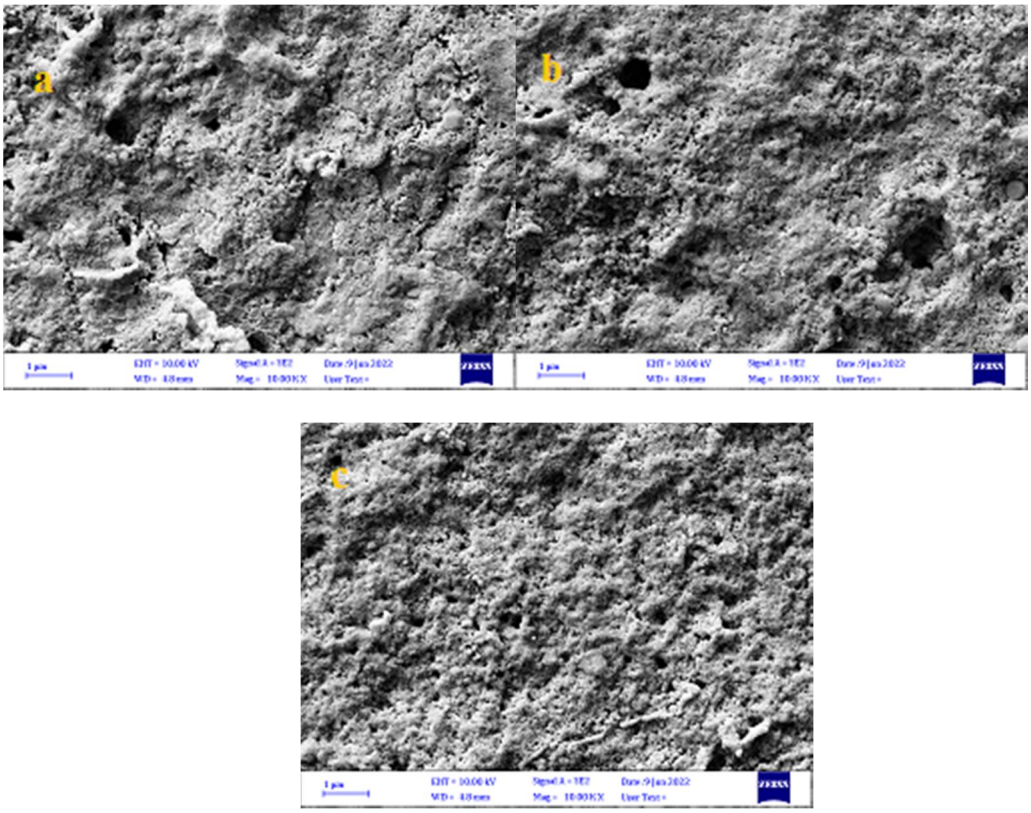

FIG. 5. The FESEM image of the surface for ZnO all layers.

Figures 6, 7, and 8 show the gas sensing properties when the thin films were exposed to the surrounding air. The conduction band electrons on the film's surface were grabbed by oxygen molecules that were adsorbed there [38]. Consequently, a depletion zone developed close to the surface, increasing the film's resistance [39]. Eqs. (1) and (2) show that when reducing gases, such as ammonia, were added to all layers of thin ZnO, they reacted with the adsorbed oxygen species.

$$O_2 + e^- \rightarrow O_{2(ads)} \quad (1)$$

$$NH_3 + 3O^-_{2(ads)} \rightarrow 2N_2 + 6H_2O + 6e^- \quad (2)$$

Due to the reducing nature of NH_3, the ZnO film's surface resistance was reduced by the interaction of ammonia molecules with the oxygen-adsorbed ZnO surface. When NH_3 entered the detecting chamber, the resistance of the thin ZnO film quickly decreased, leading to a quick rise in sensor response. When the NH_3 flow was stopped, the resistance increased, causing the response sensor to progressively return to its initial levels. Figures 6-8 show how resistance affected sensitivity for thin ZnO films with three, five, and seven layers at a 50 ppm ammonia concentration. The sensitivity (S%) of the ZnO films was calculated using Eq. (3) [40]:

$$S\% = \frac{R_a - R_g}{R_g} * 100\% \quad (3)$$

where R_a and R_g are resistances in air and testing gas, respectively.

The increased number of layers led to a higher sensor response, as shown in Figs. 6-8. Table 2 indicates that the maximum sensor response (35.81%) was attained at room temperature when there were seven layers. This is caused by a decrease in grain size and an increase in surface roughness of the thin film, with a response time of 14.4 s and a recovery time of 9.4 s, as indicated in Table 2. Additionally, we observed that throughout all samples, the sensitivity increased as the operating temperature rose, peaking at 140.7 at 150℃ for the seven-layer film. The reason for this is that the grain size has decreased and the surface roughness has increased, as shown in Fig. 8. This is crucial for determining how surface roughness and grain size affect the development of highly sensitive ZnO ammonia sensors.

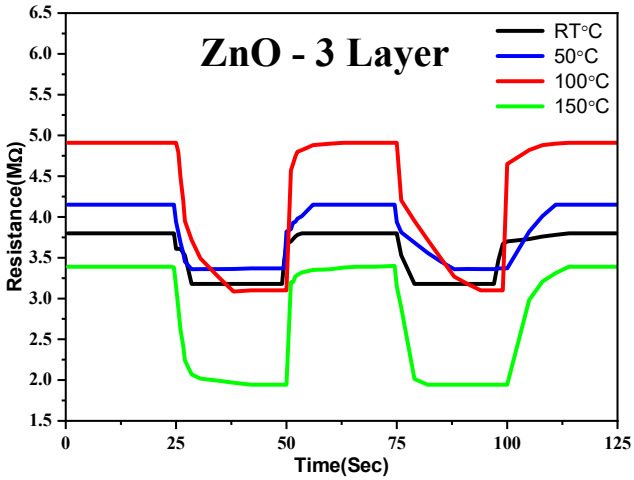

FIG. 6. Sensitivity of 3 layers of ZnO nanoparticles to 50 ppm ammonia as a function of resistance.

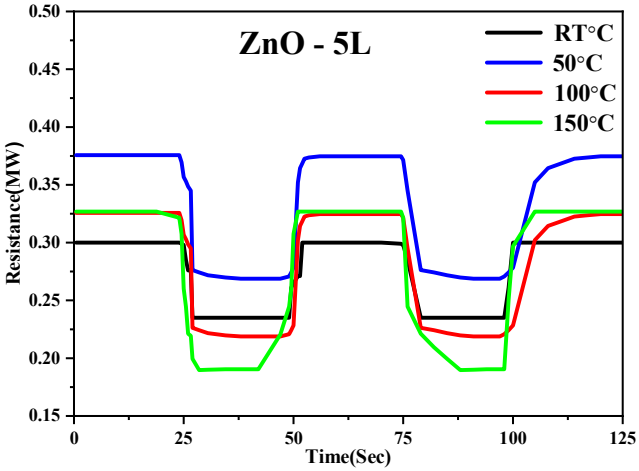

FIG. 7. Sensitivity of 5 layers of ZnO nanoparticles to 50 ppm ammonia as a function of resistance.

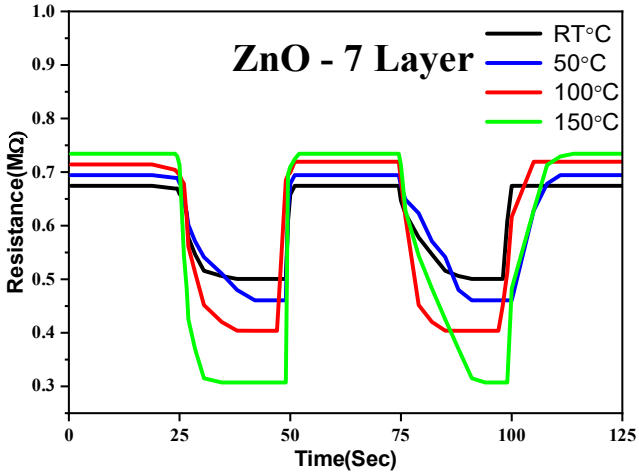

FIG. 8. Sensitivity of 7 layers of ZnO nanoparticles to 50 ppm ammonia as a function of resistance.

TABLE 2. ZnO sensitivity, response, and recovery time at layers 3, 5, and 7.

Samples	response time (s)				recovery time (s)				sensitivity (S%)			
	RT	50	100	150	RT	50	100	150	RT	50	100	150
3 La.	12.21	11.9	11.44	14.95	13.88	16.54	15.5	10.44	19.6	23.4	58.7	75.3
5 La.	8.43	12.7	11.6	9.65	13.76	13.34	12.7	14.95	27.8	39.9	47.6	76.7
7 La.	14. 4	13.9	12.22	9.6	9.4	8.53	8.32	9.56	35.8	51.7	73.3	140.7

Conclusions

Using the spin coating technique, ZnO thin films were produced for use as NH_3 gas sensors at room temperature and at operating temperatures of 50, 100, and 150 °C. The study examined how surface roughness and grain size affect ZnO films by varying the number of layers and concentration (50 ppm). The ZnO films with 3, 5, and 7 layers had the highest sensitivity small grains exhibited, which rose with an increase in working temperature. At 150 °C, the created sensor can be used to gas monitoring concentrations below 50 ppm. Films with small grains recovered faster than those with larger grains, even though they reacted to ammonia exposure more slowly. The recovery time and response time were both within 10 s. The outcomes showed that the synthesis of ZnO ammonia sensors using room-temperature spin-coating deposition was feasible, and that ZnO capacity to detect ammonia is significantly impacted by adjusting grain size to operating temperature. Consequently, it is thought that results could offer useful direction for upcoming industrial applications in the development of high-performance gas sensors.

Acknowledgements

The electronics laboratory at the College of Education of Pure Science, University of Anbar.

Funding Declaration

No funding was received for this work

Data Availability Statement

All data are available if requested by the reviewers. External data inferred within the manuscript are cited in the references.

Conflict of interest:

The authors have no conflicts to disclose.

Ethics Approval:

Ethics approval not required.

Author Contribution Declaration:

Ahmad Z. Al-Jenaby: Conceptualization, data duration, formal analysis, investigation, methodology, software, supervision, validation, visualization, writing – original draft, writing review & editing. Othman. A. Fahad: investigation, methodology، supervision, validation, and writing – original draft. Saadallah F. Hasan: writing– review & editing.

References

[1] Kuo, S.-Y., Chen, W.-C., and Cheng, C.-P., Superlattices Microstruct., 39 (1-4) (2006) 162.

[2] Banerjee, A. et al., Thin Solid Films, 496 (1) (2006) 112.

[3] Sivaramakrishnan, K. and Alford, T., Appl. Phys. Lett., 96 (20) (2010).

[4] Rwenyagila, E.R. et al., J. Mater. Res., 29 (24) (2014) 2912.

[5] Alzamzoum, T. et al., Jordan J. Phys., 17 (5) (2024) 577.

[6] Minami, T., Semicond. Sci. Technol., 20 (4) (2005) S35.

[7] Basyooni, M.A., Eker, Y.R., and Yilmaz, M., Superlattices Microstruct., 140 (2020) 106465.

[8] Korotcenkov, G., Mater. Sci. Eng. R Rep., 61 (1-6) (2008) 1.

[9] Xu, C. et al., Sens. Actuators B Chem., 3 (2) (1991) 147.

[10] Wang, X., Yee, S.S., and Carey, W.P., Sens. Actuators B Chem., 25 (1-3) (1995) 454-457.

[11] Bezy, N.A. et al., Jordan J. Phys., 17 (2) (2024) 245.

[12] Villanueva, Y.Y., Liu, D.-R., and Cheng, P.T., Thin Solid Films, 501 (1-2) (2006) 366.

[13] Fahad, O.A., Ramizy, A., and Al-Rawi, B.K., J. Mater. Sci. Mater. Electron., 35 (27) (2024) 1822.

[14] Al-Rashid, S.N.T., Nanosci. Technol. Int. J., 15 (3) (2024).

[15] Fahad, O.A., J. Opt., 2024 (2024) 1.

[16] Tamil Illakkiya, J. et al., Emerg. Mater. Res., 5 (1) (2016) 57.

[17] Rao, T.P. and Santhoshkumar, M., Appl. Surf. Sci., 255 (8) (2009) 4579.

[18] Tang, H. et al., J. Mater. Sci., 44 (2) (2009) 563.

[19] Al-Jenaby, A.Z., Al-Samarai, A.-M.E., and Ramizy, A., Mater. Today Proc., 42 (2021) 2840.

[20] Seto, J.Y., J. Electrochem. Soc., 122 (5) (1975) 701.

[21] Knuyt, G. et al., Phys. Status Solidi B, 195 (1) (1996) 179.

[22] Barna, P. and Adamik, M., Thin Solid Films, 317 (1-2) (1998) 27.

[23] Hasan, S.F. et al., IOP Conf. Ser. Mater. Sci. Eng., IOP Publishing, (2021).

[24] Fahad, O.A. et al., Sens. Actuators A Phys., 383 (2025) 116198.

[25] Kakati, N. et al., Thin Solid Films, 519 (1) (2010) 494.

[26] Al-Jenaby, A.Z., Ramizy, A., and Al-Samarai, A.-M.E., AIP Conf. Proc., AIP Publishing, (2022).

[27] Lee, J.H. et al., Nanotechnology, 20 (39) (2009) 395704.

[28] Hasan, S.F. et al., J. Opt., 2024 (2024) 1.

[29] Roy, S. and Basu, S., Bull. Mater. Sci., 25 (2002) 513.

[30] Mustafa, A. and Al-Rashid, S., Chalcogenide Lett., 21 (5) (2024) 407.

[31] Abdalameer, N.K., Fahad, O.A., and Khalaph, K.A., Int. J. Nanosci., 21 (01) (2022) 2150062.

[32] Fahad, O.A. et al., Int. J. Nanosci., 20 (06) (2021) 2150055.

[33] Al-Rawi, B.K. and Mazhir, S.N., Int. J. Nanosci., 22 (05) (2023) 2350044.

[34] Ennaceri, H. et al., Sol. Energy Mater. Sol. Cells, 201 (2019) 110058.

[35] Pankove, J.I., "Optical processes in semiconductors", (Courier Corporation, 1975).

[36] Hasan, S.F. et al., AIP Conf. Proc., AIP Publishing, (2022).

[37] Abed, H.A., Al Rashid, S.N., and Mazhir, S.N., Int. J. Nanosci., 22 (06) (2023) 2330005.

[38] Mohammed, A.S. and Fahad, O.A., AAIP Conf. Proc., AIP Publishing, (2021).

[39] Al-Jenaby, A.Z., Ramizy, A., and Al-Samarai, A.-M.E., IOP Conf. Ser. Mater. Sci. Eng., IOP Publishing, (2021).

[40] Barsan, N. and Weimar, U., J. Electroceram., 7 (2001) 143.